Nano Res (2009) 2: 565–574
DOI 10.1007/s12274-009-9056-1
Research Article

Shape-Controlled Synthesis of Octahedral α-$NaYF_4$ and Its Rare Earth Doped Submicrometer Particles in Acetic Acid

Li Gao[1,2], Xin Ge[1], Zhanli Chai[1,2], Guohai Xu[1,2], Xin Wang[3] (✉), and Cheng Wang[1] (✉)

[1] State Key Laboratory of Rare Earth Resource Utilization, Changchun Institute of Applied Chemistry, Changchun 130022, China
[2] Graduate School of the Chinese Academy of Sciences, Beijing 100049, China
[3] Division of Chemical and Biomolecular Engineering, Nanyang Technological University, Singapore 637459

Received: 29 March 2009 / Revised: 22 April 2009 / Accepted: 10 May 2009

ABSTRACT

Submicrometer sized pure cubic phase, Eu^{3+} doped, and Yb^{3+}/Er^{3+} co-doped α-$NaYF_4$ particles with octahedral morphology have been prepared in acetic acid. The acetate anion plays a critical role in the formation of such symmetric octahedral structures through its selective adsorption on the (111) faces of the products. The size of the as-prepared octahedra can be tuned by varying the amount of sodium acetate added to the acetic acid. A possible formation mechanism for these octahedra has been proposed. The doped α-$NaYF_4$ octahedral submicrometer particles show down-conversion and up-conversion photoluminescence typical of these materials.

KEYWORDS

α-$NaYF_4$, octahedral, acetic acid, photoluminescence

Introduction

Since many physical properties and potential applications of nanostructured materials are dependent on their morphologies and particle sizes [1–5], in the past several years many research efforts have been made toward the controlled synthesis of nanostructured materials with specific morphology and narrow size distribution. The optical properties of many nanoscaled semiconductors [6–9] and noble metals [10–14] can be tuned by varying their particle sizes and morphologies. However, for rare earth based luminescent materials, whose electron transitions occur within the 4f orbitals of rare earth elements which are shielded by their outer orbitals [15], any control over particle size and morphology can barely alter their optical properties. Even so, the synthesis of rare earth based luminescent materials with controlled morphologies and narrow size distribution could be important in terms of fabricating devices such as field emission displays and plasma display panels via bottom-up approaches taking advantage of their superior luminescent properties [16].

Rare earth inorganic compounds such as oxides [17–20], phosphates [21, 22], fluorides [23–25], vanadates [26], and orthoborates [27] have potential applications in high-performance magnets, optics,

Address correspondence to Cheng Wang, cwang@ciac.jl.cn; Xin Wang, WangXin@ntu.edu.sg

Springer

optoelectronics, biological labeling and catalysis [28–30] because of their unique properties arising from their 4f electron configurations. Among them, the ternary metal fluoride $NaYF_4$ has been demonstrated to be the most effective host matrix for up-conversion (UC) and down-conversion (DC) phosphors due to its low vibrational energy and high refractive index [31]. To achieve these phosphors, it is necessary to substitute Y^{3+} by other rare earth ions having appropriate numbers of 4f electrons to facilitate f–f transitions upon excitation [32, 33]. Fortunately, this can be readily fulfilled as the Y^{3+} ion in the crystal lattice of α-$NaYF_4$ can be replaced by other rare earth ions in nearly any ratio [15].

Monodispersed $NaYF_4$ and $NaYF_4$-based UC nanoparticles with controlled sizes and morphologies have been successfully prepared and reported previously [24, 25, 32–35]. Most of the UC nanoparticles were synthesized in organic solvents at high temperature [24, 36, 37] or in aqueous solutions [29, 38, 39] in the presence of organic additives. In the latter case, ethylenediaminetetraacetic acid (EDTA) [29, 40] and trisodium citrate [38, 41] have mainly been used as chelating ligands and their different chelating properties resulted in various morphologies [29, 32, 38, 40]. In the present work, we report the synthesis of octahedral α-$NaYF_4$ and its rare earth doped submicrometer particles in acetic acid. The effects of varying the reaction parameters have been systematically investigated.

1. Experimental

1.1 Synthesis

Rare earth oxides RE_2O_3 (RE=Y, Yb, Er, Eu) (99.95%) were purchased from Shanghai Yuelong New Materials Co., Ltd. Other chemicals were purchased from Beijing Chemical Co. All chemicals were used as received. Rare earth chloride stock solutions of concentration 0.5 mol/L were prepared by dissolving the corresponding metal oxides in hydrochloric acid at elevated temperature. In a typical synthesis, 0.3 mL of YCl_3 (0.5 mol/L) aqueous solution was added to a three-necked flask containing 10.0 mL glacial acetic acid and the flask was magnetically stirred throughout the synthesis. After stirring for 5.0 min, 0.7 mL of 1.0 mol/L NaF aqueous solution was added. The mixture was kept stirring for another 3.0 min, heated to the boiling point (about 106 °C) within 10.0 min and then refluxed for 1.0 h. After reaction, the flask was cooled to room temperature naturally and the precipitate was collected after centrifugation and washing with deionized water and ethanol. The products were dried at 50 °C. The same synthetic protocol was applied in the synthesis of $NaYbF_4$, $NaYF_4$:20%Yb/2%Er, and $NaYF_4$:5%Eu by substituting YCl_3 with corresponding molar ratios of $RECl_3$ (RE=Yb, Er and Eu).

1.2 Characterization

Powder X-ray diffraction (XRD) measurements were performed on a Bruker D8 Focus diffractometer with Cu Kα radiation and a Linux detector at a scanning rate of 15°/min in the 2θ range 20° to 80°. Field emission scanning electron microscopy (FESEM) images were taken using a Hitachi S-4800 microscope operated at an accelerating voltage of 10 kV. Energy dispersive X-ray analysis (EDX) was obtained on Bruker Quantax 200 attached to the microscope. Transmission electron microscopy (TEM) was performed using a JEOL-3010 instrument operated at 200 kV. Infrared spectra were measured on a Vertex 70 FT-IR spectrophotometer (Bruker) with the KBr pellet technique. For photoluminescence studies, both excitation and emission spectra were recorded with a Hitachi F-4500 spectrophotometer equipped with a 150 W Xenon lamp as the excitation source. The UC emission spectra were obtained using a 980 nm laser from a diode laser (BWT Beijing Ltd.) as the excitation source and detected by an R955 photomultiplier tube (Hamamatsu) from 450 to 700 nm.

2. Results and discussion

2.1 Characterization of typical α-$NaYF_4$ nanostructures

The XRD pattern (Fig. 1(a)) showed that pure cubic α-$NaYF_4$ phase (JCPDS card, No. 77-2042) was prepared in our typical process. FESEM results (Fig. 1(b)) revealed that the product consists of octahedral

submicrometer particles. The edge length of each octahedron lies in the range 100 to 200 nm and the average length is about 180 nm. Meanwhile, the surface of the octahedral particles, seen by closer observation under higher magnification of FESEM as shown in the inset of Fig. 1(b), is fairly smooth. Under TEM observation (Fig. 1(c)), the octahedral particles are still discernible although some particles look like parallelograms in shape as a result of the 2-D projection. The diffraction spots of the SAED pattern (inset of Fig. 1(c)) are indexed to the (111) and (200) planes of α-$NaYF_4$. The HRTEM image (Fig. 1(d)) displays an interplanar distance of 0.31 nm, which can be ascribed to the lattice spacing of the (111) planes of α-$NaYF_4$. These results suggest the high crystallinity of the as-prepared α-$NaYF_4$.

We found that the qualities of the final product including the crystallinity and geometric shape were strongly dependent to the synthesis conditions. Deviations from the optimized typical conditions led to dramatic changes in these properties.

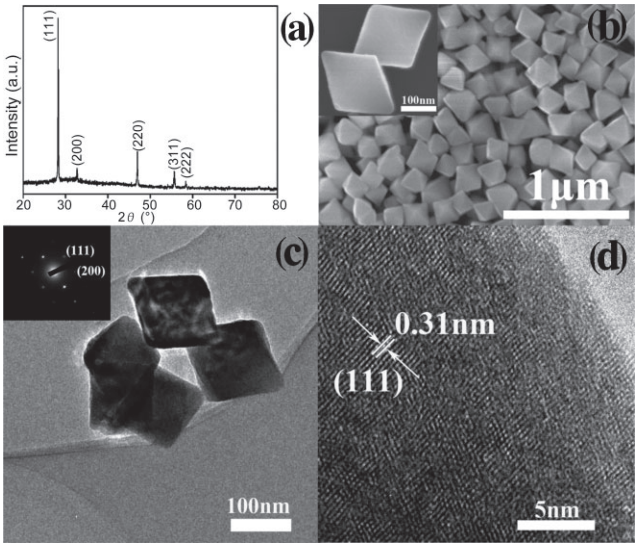

Figure 1 (a) XRD pattern, (b) FESEM image, (c) TEM image, and (d) HRTEM image of octahedral α-$NaYF_4$ prepared in the typical synthetic process

2.2 Effects of varying the amount of NaF

The effects of the added amount of 1.0 mol/L NaF aqueous solution on the morphology and chemical composition of α-$NaYF_4$ submicrometer particles were studied by varying its volume in the range 0.3 to 2.0 mL while keeping the other parameters unchanged. The optimum volume of 1.0 mol/L NaF aqueous solution was found to be 0.7 mL with a corresponding F^- to Y^{3+} molar ratio of 14/3. When the volume was less than 0.7 mL, XRD results (not shown) indicated that poorly crystalline YF_3 and unknown impurities were also produced besides α-$NaYF_4$. Larger volumes of NaF aqueous solution favored the formation of pure α-$NaYF_4$. Furthermore, the morphology also varied with the volume of NaF aqueous solution added as shown in Fig. 2. When the volume was 0.3 mL, pancake-like particles with dimensions around 100 nm were the major product (Fig. 2(a)). On increasing the volume to 0.6 mL, two kinds of morphologies were observed (Fig. 2(b)). One was a leaf-like product, which might be amorphous as a pure α-$NaYF_4$ phase was the only crystalline product observable by XRD. The other one was octahedral in shape and believed to be α-$NaYF_4$.

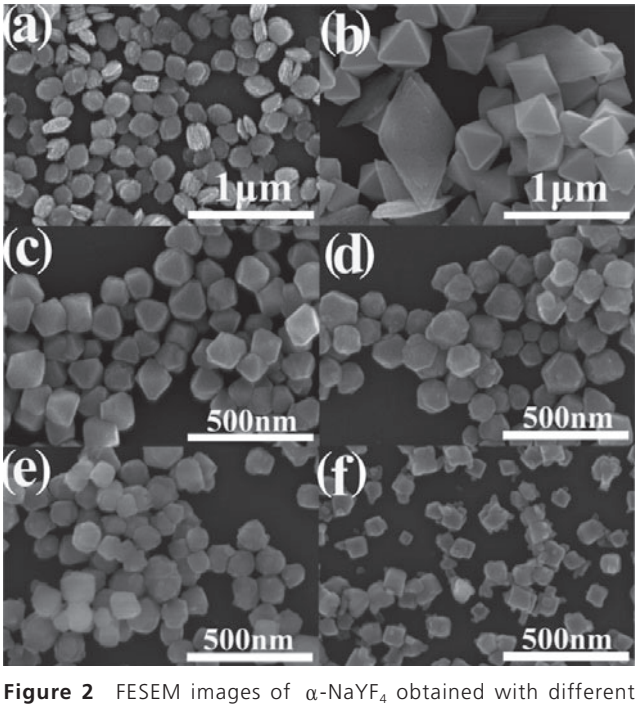

Figure 2 FESEM images of α-$NaYF_4$ obtained with different volumes of 1.0 mol/L NaF aqueous solution: (a) 0.3 mL, (b) 0.6 mL, (c) 0.8 mL, (d) 0.9 mL, (e) 1.0 mL, and (f) 2.0 mL. Volume of 0.5 mol/L YCl_3: 0.3 mL, volume of acetic acid: 10.0 mL, reaction temperature: 106 °C, reaction time: 1 h

When the volume was larger than 0.8 mL, the particle sizes tended to decrease with the increase in volume of NaF. Meanwhile, the six vertexes of the α-$NaYF_4$ octahedra become less prominent as shown in Figs.

2(c) and 2(d) and the surfaces of octahedra became roughened. On further increasing the volumes to 1.0 and 2.0 mL, the morphology evolved into cuboid structures with sizes less than 100 nm (Figs. 2(e) and 2(f)) coexisting with some small irregular nanoparticles.

2.3 Effects of water

In our typical process, only the water from the aqueous solutions of the two precursors was added to the reaction system. When the two reagents (solid YCl_3 and glacial acetic acid) were used as source materials instead of their corresponding aqueous solutions, only poorly crystalline products could be obtained and the yield was extremely low (Fig. S-1(a) in the Electronic Supplementary Material (ESM)). On the other hand, without the use of acetic acid, irregular α-$NaYF_4$ particles were produced in 10.0 mL of water (Fig. S-1(b) in the ESM). However, if 1.0 or 2.0 mL of water was added to 10.0 mL of acetic acid *prior to* the addition of the aqueous solutions of the two precursors, along with octahedral (FESEM) α-$NaYF_4$ (XRD results not shown) particles, an unknown phase with a stick-like morphology was produced (Figs. S-1(c) and S-1(d) in the ESM). The percentage of octahedral particles decreased with increasing volume of water. A summary of the effect of water on the synthesis is also provided in Table S-1 (in the ESM). Interestingly, the adverse effect of extraneous water could be compensated by adding sodium acetate (NaOAc) to the reaction system. For example, when 1.0 mL of water was replaced by 1.0 mL of 1.0 mol/L NaOAc, similar octahedral nanoparticles with smaller particle sizes were obtained (Fig. S-1(e) in the ESM). It was also found that adding more NaOAc aqueous solution to the system did not lead to a change in crystal phase from α-$NaYF_4$, but it did alter the morphology from octahedral to an irregular shape (Fig. S-1(f) in the ESM).

2.4 Effect of NaOAc

When solid NaOAc was added to 10.0 mL of acetic acid prior to reaction and the other conditions remained unchanged, it was found that smaller octahedra were obtained. In addition, the yield of α-$NaYF_4$ decreased with increasing the amount of NaOAc. Figure 3(a) shows that the particle size was about 110 nm when 0.24 mmol of NaOAc was added. On increasing the amount of NaOAc to 0.48 mmol, the particle size decreased to about 50 nm (Fig. 3(b)) and it was also found that the particles became more uniform. However, on further increasing the amount of NaOAc to 0.72 or 0.96 mmol, no significant variation of morphology was observed but the yields of α-$NaYF_4$ decreased.

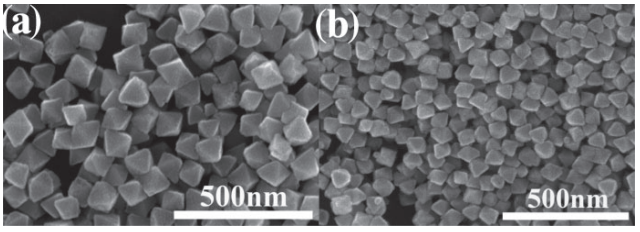

Figure 3 FESEM images of α-$NaYF_4$ obtained with different amounts of NaOAc added to the reaction system: (a) 0.24 mmol, and (b) 0.48 mmol. Volume of 0.5 mol/L YCl_3: 0.3 mL, volume of 1.0 mol/L NaF: 0.7 mL, volume of acetic acid: 10.0 mL, reaction temperature: 106 °C, reaction time: 1 h

2.5 Effects of reaction duration and temperature

Generally, the octahedral α-$NaYF_4$ was not well developed when the reaction time was less than 1.0 h (Fig. S-2(a)), indicating that the reaction was incomplete. Prolonging the reaction time beyond 1.0 h to 5.0 h and even 12.0 h had little effect on the quality of the product. Reaction temperature was found to play a key role in the formation of octahedral α-$NaYF_4$ particles. On lowering the temperature to 95 °C, the octahedral particles were poorly developed, with missing vertexes and the surfaces were covered by small nanoparticles (Fig. S-2(b) in the ESM). This is similar to the effect of reduced reaction time. Reactions at even lower temperature, e.g., 85 °C, afforded only small amounts of poorly crystalline agglomerated nanoparticles (Fig. S-2(c) in the ESM). We noticed that increasing the amount of added NaF aqueous solution favored the formation of α-$NaYF_4$ in our system as mentioned above. By adding 3.5 mL of NaF (1.0 mol/L) aqueous solution to 10 mL acetic acid, decreasing the reaction temperature to 40 °C and prolonging the reaction time to 12.0 h, nearly cuboid structures with an average size of about 120 nm were produced (Fig. S-2(d) in the ESM). XRD revealed

that the cuboid product is still α-$NaYF_4$. Careful examination under high magnification FESEM images showed that it consists of smaller nanoparticles with size below 20 nm.

In this paper, our goal is to use symmetrical submicrometer sized α-$NaYF_4$ particles as host material for Eu^{3+} doping or Yb^{3+}/Er^{3+} co-doping. Preliminary optical investigations showed that the cuboid $NaYF_4$ particles are a poor host material in terms of photoluminescence properties for corresponding 5% Eu^{3+} doped $NaYF_4$ and 20% Yb^{3+}/2% Er^{3+} co-doped α-$NaYF_4$. This might be due to there being too many defects originating from the constituent nanoparticles. Therefore, no attempt has been made to optimize the synthesis of this particles with this cuboid morphology.

2.6 Formation mechanism of the octahedral submicrometer particles

Similar to other symmetrical nanostructured materials including noble metals [42–44], Cu_2O [45–47], and lead chalcogenides [8, 48, 49], the surface of the octahedral α-$NaYF_4$ is believed to be enclosed by (111) facets. α-$NaYF_4$ has a structure isomorphous with the fluorite (CaF_2) structure in which Ca^{2+} sites have been replaced randomly by Na^+ and Y^{3+} cations and the two metal cations fit into the tetrahedral holes formed by the fluoride anions. As shown in Fig. 4, the atomic arrangements on different crystalline planes are quite different. The (100) planes are built up from F–M double layers (Fig. 4(a)) while the (110) and (111) planes are built up from MF_2 (Fig. 4(b)) single layers and F–M–F triple layers (Fig. 4(c)), respectively. Noting that the acetate anion has significant effects on the morphology of the submicrometer α-$NaYF_4$ particles in our system, it is suggested that the surface energy of a specific crystalline plane might be reduced by the adsorption of acetate anions via electrostatic interactions with the metal cations. The presence of acetate ions in the octahedral α-$NaYF_4$ submicrometer particles was verified by FTIR spectroscopy (not shown). The extent of reduction in surface energy might be correlated with the metal atom density of each surface within the fluorite structure, which follows the order (111) > (100) > (110). This implies that the metal cations on (111) faces of α-$NaYF_4$ are likely to be blocked by acetate anions and the surface energy of such faces would be decreased more significantly. Thus, the (100) faces become the highest energy surface with the fastest growth rate. Initially, cuboid nuclei of α-$NaYF_4$ with (100) faces that mirror its crystal nature were formed. The six (100) faces tend to grow and form nanostructures with six pods. The rough surfaces of the six pods, which are presumed to have plenty of kinks, would be filled with constituents within the reaction system. Partially filled surfaces lead to the formation of hopper morphologies, which are characterized by step-wise depressed centers of faces due to the high growth rates at edges or corners [50, 51]. When the depressed surfaces are fully filled, an octahedron enclosed by acetate-blocked (111) facets would evolve and further growth of particles would be terminated. A scheme for the possible growth of octahedral

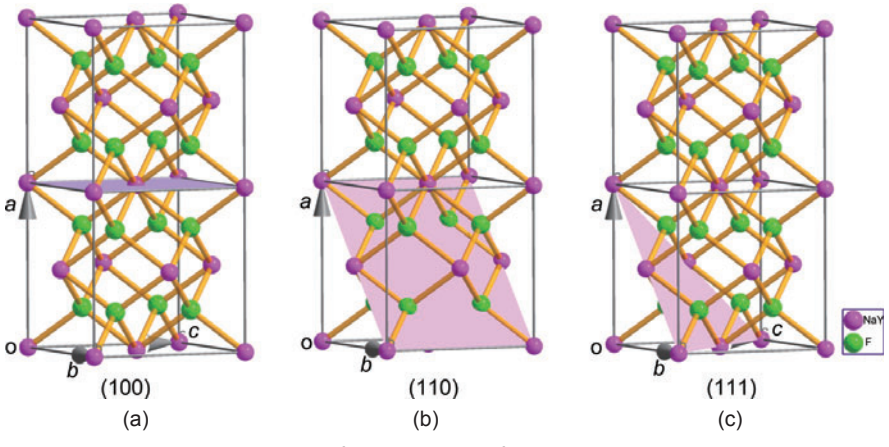

Figure 4 Schematic illustration of the structure of cubic α-$NaYF_4$. The shaded crystalline planes are (a) (100), (b) (110), and (c) (111)

α-$NaYF_4$ submicrometer particles is presented in Fig. S-3 (in the ESM). Unfortunately, we did not observe any star-shaped nanostructures with six pods in our process because of the high degree of supersaturation within the reaction system [48]. However, we did obtain octahedral α-$NaYF_4$ submicrometer particles with depressed surfaces as shown in Fig. S-2(a) (in the ESM) when the reaction time was limited to 30 min. Furthermore, the natural cleavage plane for the fluorite structure is its (111) surface [52]. This might serve as a additional factor in stabilizing the octahedral morphology beside the aforementioned surface energy reduction of (111) faces by adsorbed acetate anions.

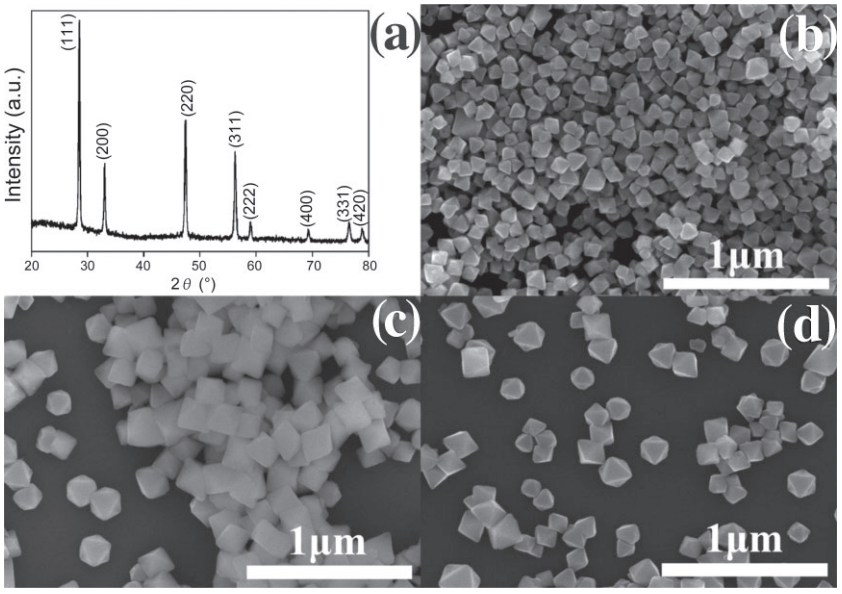

Figure 5 (a) XRD pattern and (b) FESEM image of as-prepared α-$NaYbF_4$; FESEM images of as-prepared (c) α-$NaYF_4$:5%Eu^{3+} and (d) α-$NaYF_4$:20%Yb^{3+}/2%Er^{3+}. Total volume of 0.5 mol/L $RECl_3$ (RE = Y, Yb, Eu, Er): 0.3 mL, volume of 1.0 mol/L NaF: 0.7 mL, volume of acetic acid: 10.0 mL, reaction temperature: 106 °C, reaction time: 1.0 h

Our experimental results also showed that NaOAc is superior to NaF in terms of reducing the particle size of the final products. This could be due to the fact that the growth habit along the axes of different crystalline faces was maintained throughout the synthetic course when NaOAc was used. In this case, the molar ratio of F^-/Y^{3+} remained unchanged, whereas this was obviously not the case when increasing the volume of NaF aqueous solution.

2.7 Photoluminescence properties

As an efficient host lattice for DC and UC materials, the optical properties of $NaYF_4$ can be improved via doping with other rare earth elements. To make sure that such doping did not cause dramatic changes of both crystal structure and morphology, the validity of our synthetic protocol was firstly tested by fully replacing Y^{3+} with Yb^{3+}. XRD and FESEM results showed that the cubic phase of $NaYbF_4$ (JCPDS card, No. 77-2043) with octahedral morphology can also be obtained (Figs. 5(a) and 5(b)). The main difference between the two products was that the average particle size of $NaYbF_4$, 110 nm, was less than that of α-$NaYF_4$ obtained under same conditions. Extension of this method to the synthesis of $NaYF_4$:5%Eu and $NaYF_4$:20%Yb/2%Er also proved to be successful as confirmed by their XRD patterns (not shown) and FESEM images (Figs. 5(c) and 5(d)). The reason for only doping α-$NaYF_4$ submicrometer particles obtained via our typical synthesis process is that larger particles with fewer defects and better optical properties were obtained under these conditions. Meanwhile, the selection of rare earth ions and their replacement percentages are in accordance with the literature as they have been well established in previous studies [53]. The calculated lattice parameters for fully replaced Yb^{3+}, partially doped Eu^{3+} and Yb^{3+}/Er^{3+} co-doped samples are summarized in Table 1. The difference between these parameters can be interpreted using Vegard's rule [54]. The particle size of the Eu doped product remains nearly unchanged and the percentages of Y and Eu in this

Table 1 The calculated lattice parameters of octahedral $NaYF_4$, $NaYF_4$:5%Eu, $NaYF_4$:20%Yb/2%Er, and $NaYbF_4$

Product	Calculated lattice parameter (Å)
$NaYF_4$	5.469
$NaYF_4$:Eu	5.476
$NaYF_4$:Yb/Er	5.458
$NaYbF_4$	5.415

product are 95.24% and 4.76%, respectively, as given by EDX analysis (Fig. S-4(a) in the ESM) and are close to the nominal molar ratio. For Yb^{3+}/Er^{3+} co-doped α-$NaYF_4$, it was found that the particle size varied from 80 to 180 nm and the molar ratio of Y:Yb:Er (83.42:13.96:2.62, Fig. S-4(b) in the ESM) deviated somewhat from the nominal value (78.0:20.0:2.0).

2.7.1 $NaYF_4:Eu^{3+}$

Figure 6 presents the room temperature photoluminescence excitation (a) and emission (b) spectra of the resulting $NaYF_4$:5% Eu^{3+} phosphors. From Fig. 6(a), we can see that the excitation spectrum consists of the characteristic excitation lines of Eu^{3+} within its $4f^6$ configuration from 200 to 500 nm. Most of the excitation lines can be clearly assigned (321 nm, $^7F_0 \rightarrow {}^5H_6$; 364 nm, $^7F_0 \rightarrow {}^5D_4$; 382 nm, $^7F_0 \rightarrow {}^5G_2$; 396 nm, $^7F_0 \rightarrow {}^5L_6$; 418 nm, $^7F_0 \rightarrow {}^5D_3$; 466nm, $^7F_0 \rightarrow {}^5D_2$). The other weak excitation lines at 253, 271, 288, and 300 nm which have little contribution to the excitation of Eu^{3+} are of minor significance. The emission spectra (Fig. 6(b)), excited using 396 nm UV light, consist of emission lines associated with the Eu^{3+} transitions from the excited $^5D_{0-2}$ levels to the ^7F_J level, that is, 509 nm, $^5D_2 \rightarrow {}^7F_3$; 525 nm, $^5D_1 \rightarrow {}^7F_0$; 534 nm, $^5D_1 \rightarrow {}^7F_1$; 554 nm, $^5D_1 \rightarrow {}^7F_2$; 590 nm, $^5D_0 \rightarrow {}^7F_1$; 612 nm, $^5D_0 \rightarrow {}^7F_2$; 650 nm, $^5D_0 \rightarrow {}^7F_3$; 693 nm, $^5D_0 \rightarrow {}^7F_4$. Of these, the strongest emission is $^5D_0 \rightarrow {}^7F_1$ at 590 nm.

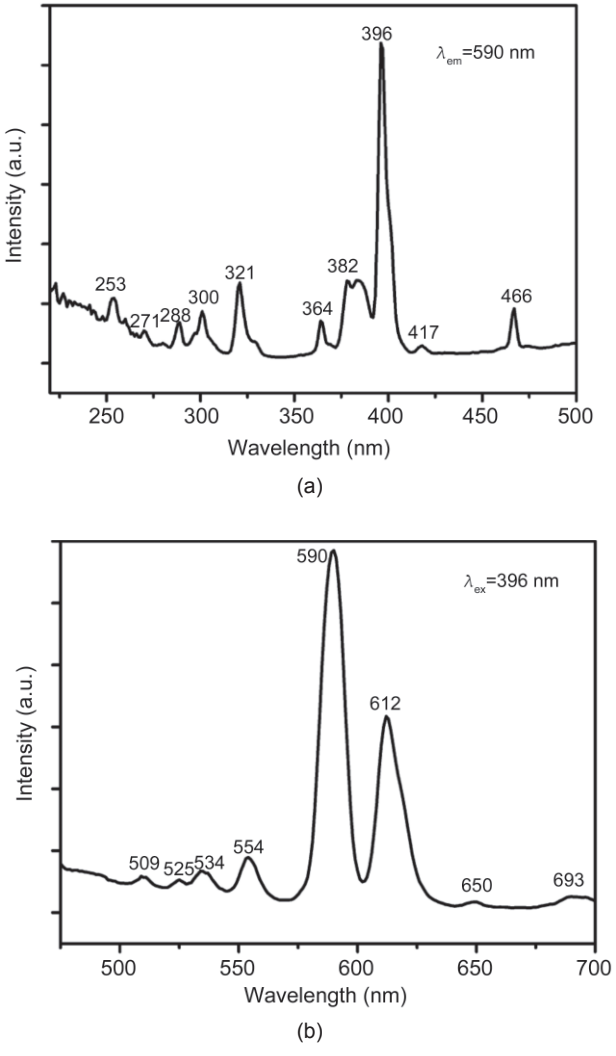

Figure 6 Photoluminescence excitation (a) and emission (b) spectra of α-$NaYF_4$:5%Eu^{3+}

2.7.2 $NaYF_4:Yb^{3+}/Er^{3+}$

The pathways of UC excitation for Er^{3+}/Yb^{3+} ion couples in rare earth fluoride have been extensively studied [15, 34]. Figure 7 shows the UC emission spectra of $NaYF_4$:Yb^{3+}/Er^{3+} under a 980 nm laser source. There are three emission bands located at around 525, 547, and 660 nm which can be assigned to the $^2H_{11/2} \rightarrow {}^4I_{15/2}$, $^4S_{3/2} \rightarrow {}^4I_{15/2}$, and $^4F_{9/2} \rightarrow {}^4I_{15/2}$ transitions of Er^{3+}. The broadening of the latter two peaks can be ascribed to the splitting of the energy levels of Er^{3+} caused by the electrical field created by the surrounding $NaYF_4$ host material, a well known process called Stark splitting [55]. The UC emission spectra also indicate that the red emission is the strongest among the three emissions [23, 41]. We believe that the cross-relaxation process between ($^4F_{7/2}$

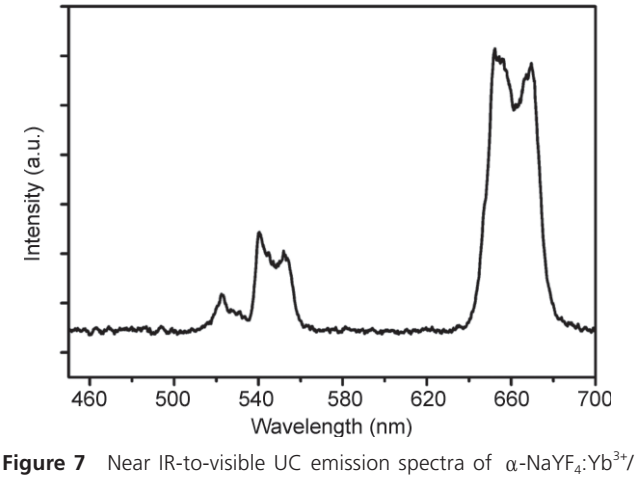

Figure 7 Near IR-to-visible UC emission spectra of α-$NaYF_4$:Yb^{3+}/Er^{3+} under 980 nm laser excitation

$\rightarrow {}^4F_{9/2}$) and ($^4F_{9/2} \leftarrow {}^4I_{11/2}$) resonant transitions occurs and leads to a decrease in the green emission and an increase in the red emission [41].

3. Conclusions

We have developed a method for the synthesis of uniform octahedral α-$NaYF_4$ particles, with size around 180 nm, in acetic acid. The influence of varying the reaction parameters on the synthesis has been investigated. Selective adsorption of OAc^- anions from acetic acid on (111) faces of α-$NaYF_4$ is believed to be the major factor in the morphology control. The optimized reaction conditions were extended to the synthesis of 5%Eu^{3+} doped and 20%Yb^{3+}/2%Er^{3+} co-doped α-$NaYF_4$ photoluminescence materials. Only slight differences in particle size were observed for the doped α-$NaYF_4$ particles, which demonstrates the validity of our synthetic protocol for preparing $NaLnF_4$ materials. Photoluminescence properties of both Eu^{3+} doped DC and Yb^{3+}/Er^{3+} co-doped UC products were consistent with literature reports.

Acknowledgements

This work is supported by the National Basic Research Program of China (2007CB925101) and National Science Foundation of China (20671087).

Electronic Supplementary Material: Supplementary material is available in the online version of this article at http://dx.doi.org/10.1007/s12274-009-9056-1 and is accessible free of charge.

References

[1] Alivisatos, A. P. Semiconductor clusters, nanocrystals, and quantum dots. *Science* **1996,** *271,* 933–937.

[2] Williams, F.; Nozik, A. J. Solid-state perspectives of the photoelectrochemistry of semiconductor electrolyte junctions. *Nature* **1984,** *312,* 21–27.

[3] Sun, S. H.; Murray, C. B.; Weller, D.; Folks, L.; Moser, A. Monodisperse FePt nanoparticles and ferromagnetic FePt nanocrystal superlattices. *Science* **2000,** *287,* 1989–1992.

[4] Bruchez, M.; Moronne, M.; Gin, P.; Weiss, S.; Alivisatos, A. P. Semiconductor nanocrystals as fluorescent biological labels. *Science* **1998,** *281,* 2013–2016.

[5] Yin, Y.; Alivisatos, A. P. Colloidal nanocrystal synthesis and the organic–inorganic interface. *Nature* **2005,** *437,* 664–670.

[6] Klarreich, E. Biologists join the dots. *Nature* **2001,** *413,* 450–452.

[7] Duan, J. L.; Song, L. X.; Zhan, J. H. One-pot synthesis of highly luminescent CdTe quantum dots by microwave irradiation reduction and their Hg^{2+}-sensitive properties. *Nano Res.* **2009,** *2,* 61–68.

[8] Peng, X. G.; Wickham, J.; Alivisatos, A. P. Kinetics of Ⅱ–Ⅳ and Ⅲ–Ⅴ colloidal semiconductor nanocrystal growth: "Focusing" of size distributions. *J. Am. Chem. Soc.* **1998,** *120,* 5343–5344.

[9] Peng, Z. A.; Peng, X. G. Formation of high-quality CdTe, CdSe, and CdS nanocrystals using CdO as precursor. *J. Am. Chem. Soc.* **2001,** *123,* 183–184.

[10] Xue, C.; Mirkin, C. A. pH-switchable silver nanoprism growth pathways. *Angew. Chem. Int. Ed.* **2007,** *46,* 2036–2038.

[11] Metraux, G. S.; Mirkin, C. A. Rapid thermal synthesis of silver nanoprisms with chemically tailorable thickness. *Adv. Mater.* **2005,** *17,* 412–415.

[12] Au, L.; Chen, Y.; Zhou, F.; Camargo, P. H. C.; Lim, B.; Li, Z. Y.; Ginger, D.; Xia, Y. N. Synthesis and optical properties of cubic gold nanoframes. *Nano Res.* **2008,** *1,* 441–449.

[13] Peng, S.; Lee, Y. M.; Wang, C.; Yin, H. F.; Dai, S.; Sun, S. H. A facile synthesis of monodisperse Au nanoparticles and their catalysis of CO oxidation. *Nano Res.* **2008,** *1,* 229–234.

[14] Kim, F.; Connor, S.; Song, H.; Kuykendall, T.; Yang, P. D. Platonic gold nanocrystals. *Angew. Chem. Int. Ed.* **2004,** *43,* 3673–3677.

[15] Kramer, K. W.; Biner, D.; Frei, G.; Gudel, H. U.; Hehlen, M. P.; Luthi, S. R. Hexagonal sodium yttrium fluoride-based green and blue emitting upconversion phosphors. *Chem. Mater.* **2004,** *16,* 1244–1251.

[16] Yu, M.; Lin, J.; Fu, J.; Zhang, H. J.; Han, Y. C. Sol–gel synthesis and photoluminescent properties of $LaPO_4$: A (A = Eu^{3+}, Ce^{3+}, Tb^{3+}) nanocrystalline thin films. *J. Mater. Chem.* **2003,** *13,* 1413–1419.

[17] Si, R.; Zhang, Y. W.; You, L. P.; Yan, C. H. Rare-earth oxide nanopolyhedra, nanoplates, and nanodisks. *Angew. Chem. Int. Ed.* **2005,** *44,* 3256–3260.

[18] Cao, Y. C. Synthesis of square gadolinium-oxide nanoplates. *J. Am. Chem. Soc.* **2004,** *126,* 7456–7457.

[19] Yu, T. Y.; Joo, J.; Park, Y. I.; Hyeon, T. Large-scale nonhydrolytic sol–gel synthesis of uniform-sized ceria nanocrystals with spherical, wire, and tadpole shapes. *Angew. Chem. Int. Ed.* **2005,** *44,* 7411–7414.

[20] Xu, A. W.; Fang, Y. P.; You, L. P.; Liu, H. Q. A simple method to synthesize $Dy(OH)_3$ and Dy_2O_3 nanotubes. *J. Am. Chem. Soc.* **2003,** *125,* 1494–1495.

[21] Buehler, G.; Feldmann, C. Microwave-assisted synthesis of luminescent $LaPO_4$:Ce, Tb nanocrystals in ionic liquids. *Angew. Chem. Int. Ed.* **2006,** *45,* 4864–4867.

[22] Riwotzki, K.; Meyssamy, H.; Schnablegger, H.; Kornowski, A.; Haase, M. Liquid-phase synthesis of colloids and redispersible powders of strongly luminescing $LaPO_4$:Ce, Tb nanocrystals. *Angew. Chem. Int. Ed.* **2001,** *40,* 573–576.

[23] Boyer, J. C.; Vetrone, F.; Cuccia, L. A.; Capobianco, J. A. Synthesis of colloidal upconverting $NaYF_4$ nanocrystals doped with Er^{3+}, Yb^{3+} and Tm^{3+}, Yb^{3+} via thermal decomposition of lanthanide trifluoroacetate precursors. *J. Am. Chem. Soc.* **2006,** *128,* 7444–7445.

[24] Mai, H. X.; Zhang, Y. W.; Si, R.; Yan, Z. G.; Sun, L. D.; You, L. P.; Yan, C. H. High-quality sodium rare-earth fluoride nanocrystals: Controlled synthesis and optical properties. *J. Am. Chem. Soc.* **2006,** *128,* 6426–6436.

[25] Liang, X.; Wang, X.; Zhuang, J.; Peng, Q.; Li, Y. D. Synthesis of $NaYF_4$ nanocrystals with predictable phase and shape. *Adv. Funct. Mater.* **2007,** *17,* 2757–2765.

[26] Huignard, A.; Buissette, V.; Laurent, G.; Gacoin, T.; Boilot, J. P. Synthesis and characterizations of YVO_4:Eu colloids. *Chem. Mater.* **2002,** *14,* 2264–2269.

[27] Li, Z. H.; Zeng, J. H.; Li, Y. D. Solvothermal route to synthesize well-dispersed YBO_3:Eu nanocrystals. *Small* **2007,** *3,* 438–443.

[28] Downing, E.; Hesselink, L.; Ralston, J.; Macfarlane, R. A three-color, solid-state, three-dimensional display. *Science* **1996,** *273,* 1185–1189.

[29] Yi, G. S.; Lu, H. C.; Zhao, S. Y.; Ge, Y.; Yang, W. J.; Chen, D. P.; Guo, L. H. Synthesis, characterization, and biological application of size-controlled nanocrystalline $NaYF_4$:Yb, Er infrared-to-visible up-conversion phosphors. *Nano Lett.* **2004,** *4,* 2191–2196.

[30] Wang, L. Y.; Li, Y. D. Green upconversion nanocrystals for DNA detection. *Chem. Commun.* **2006,** 2557–2559.

[31] Diamente, P. R.; Raudsepp, M.; van Veggel, F. C. J. M. Dispersible Tm^{3+}-doped nanoparticles that exhibit strong 1.47 μm photoluminescence. *Adv. Funct. Mater.* **2007,** *17,* 363–368.

[32] Zhuang, J. L.; Liang, L. F.; Sung, H. H. Y.; Yang, X. F.; Wu, M. M.; Williams, I. D.; Feng, S. H.; Su, Q. Controlled hydrothermal growth and up-conversion emission of $NaLnF_4$ (Ln = Y, Dy–Yb). *Inorg. Chem* **2007,** *46,* 5404–5410.

[33] Wang, L. Y.; Li, Y. D. $Na(Y_{1.5}Na_{0.5})F_6$ single-crystal nanorods as multicolor luminescent materials. *Nano Lett.* **2006,** *6,* 1645–1649.

[34] Boyer, J. C.; Cuccia, L. A.; Capobianco, J. A. Synthesis of colloidal upconverting $NaYF_4$:Er^{3+}/Yb^{3+} and Tm^{3+}/Yb^{3+} monodisperse nanocrystals. *Nano Lett.* **2007,** *7,* 847–852.

[35] Heer, S.; Kompe, K.; Gudel, H. U.; Haase, M. Highly efficient multicolour upconversion emission in transparent colloids of lanthanide-doped $NaYF_4$ nanocrystals. *Adv. Mater.* **2004,** *16,* 2102–2105.

[36] Zhang, Y. W.; Sun, X.; Si, R.; You, L. P.; Yan, C. H. Single-crystalline and monodisperse LaF_3 triangular nanoplates from a single-source precursor. *J. Am. Chem. Soc.* **2005,** *127,* 3260–3261.

[37] Wei, Y.; Lu, F. Q.; Zhang, X. R.; Chen, D. P. Synthesis of oil-dispersible hexagonal-phase and hexagonal-shaped $NaYF_4$:Yb, Er nanoplates. *Chem. Mater.* **2006,** *18,* 5733–5737.

[38] Li, C. X.; Yang, J.; Quan, Z. W.; Yang, P. P.; Kong, D. Y.; Lin, J. Different microstructures of β-$NaYF_4$ fabricated by hydrothermal process: Effects of pH values and fluoride sources. *Chem. Mater.* **2007,** *19,* 4933–4942.

[39] Tao, F.; Wang, Z. J.; Yao, L. Z.; Cai, W. L.; Li, X. G. Synthesis and photoluminescence properties of truncated octahedral Eu-doped YF_3 submicrocrystals or nanocrystals. *J. Phys. Chem. C.* **2007,** *111,* 3241–3245.

[40] Wang, Z. J.; Tao, F.; Cai, W. L.; Yao, L. Z.; Li, X. G. Controlled-synthesis and up-conversion luminescence of $NaYF_4$:Yb, Er phosphors. *Solid State Commun.* **2007,** *144,* 255–258.

[41] Sun, Y. J.; Chen, Y.; Tian, L. J.; Yu, Y.; Kong, X. G.; Zhao, J. W.; Zhang, H. Controlled synthesis and morphology dependent upconversion luminescence of $NaYF_4$:Yb, Er nanocrystals. *Nanotechnology* **2007,** *18,* 275609.

[42] Wang, X.; Zhuang, J.; Peng, Q.; Li, Y. D. A general strategy for nanocrystal synthesis. *Nature* **2005,** *437,* 121–124.

[43] Sun, Y. G.; Xia, Y. N. Shape-controlled synthesis of gold and silver nanoparticles. *Science* **2002,** *298,* 2176–2179.

[44] Seo, D.; Park, J. C.; Song, H. Polyhedral gold nanocrystals with O_h symmetry: From octahedra to cubes. *J. Am. Chem. Soc.* **2006,** *128,* 14863–14870.

[45] Li, H.; Liu, R.; Zhao, R. X.; Zheng, Y. F.; Chen, W. X.; Xu, Z. D. Morphology control of electrodeposited Cu_2O crystals in aqueous solutions using room temperature hydrophilic ionic liquids. *Cryst. Growth Des.* **2006,** *6,* 2795–2798.

[46] Gou, L. F.; Murphy, C. J. Solution-phase synthesis of Cu_2O nanocubes. *Nano Lett.* **2003,** *3,* 231–234.

[47] Gou, L. F.; Murphy, C. J. Controlling the size of Cu_2O nanocubes from 200 to 25 nm. *J. Mater. Chem.* **2004,** *14,* 735–738.

[48] Peng, Z. P.; Jiang, Y. S.; Song, Y. H.; Wang, C.; Zhang, H. J. Morphology control of nanoscale PbS particles in a polyol process. *Chem. Mater.* **2008,** *20,* 3153–3162.

[49] Houtepen, A. J.; Koole, R.; Vanmaekelbergh, D. L.; Meeldijk, J.; Hickey, S. G. The hidden role of acetate in the PbSe nanocrystal synthesis. *J. Am. Chem. Soc.* **2006,** *128,* 6792–6793.

[50] Murray, B. J.; Li, Q.; Newberg, J. T.; Menke, E. J.; Hemminger, J. C.; Penner, R. M. Shape- and size-selective electrochemical synthesis of dispersed silver(I) oxide colloids. *Nano Lett.* **2005,** *5,* 2319–2324.

[51] Siegfried, M. J.; Choi, K. S. Directing the architecture of cuprous oxide crystals during electrochemical growth. *Angew. Chem. Int. Ed.* **2005,** *44,* 3218–3223.

[52] Schultz, R. A.; Jensen, M. C.; Bradt, R. C. Single-crystal cleavage of brittle materials. *Int. J. Fract.* **1994,** *65,* 291–312.

[53] Liang, L. F.; Wu, H.; Hu, H. L.; Wu, M. M.; Su, Q. Enhanced blue and green upconversion in hydrothermally synthesized hexagonal $NaY_{1-x}Yb_xF_4:Ln^{3+}$ (Ln^{3+} = Er^{3+} or Tm^{3+}). *J. Alloy. Compd.* **2004,** *368,* 94–100.

[54] Vegard, L. The constitution of the mixed crystals and the filling of space of the atoms. *Z. Phys.* **1921,** *5,* 17–26.

[55] Lue, Q.; Guo, F. Y.; Sun, L.; Li, A. H.; Zhao, L. C. Surface modification of $ZrO_2:Er^{3+}$ nanoparticles to attenuate aggregation and enhance upconversion fluorescence. *J. Phys. Chem. C* **2008,** *112,* 2836–2844.